PAPER • OPEN ACCESS

Characterization of thin-film adhesion and phonon lifetimes in Al/Si membranes by picosecond ultrasonics

To cite this article: Martin Grossmann *et al* 2017 *New J. Phys.* **19** 053019

New Journal of Physics
The open access journal at the forefront of physics

Deutsche Physikalische Gesellschaft DPG
IOP Institute of Physics

Published in partnership with: Deutsche Physikalische Gesellschaft and the Institute of Physics

OPEN ACCESS

RECEIVED
3 February 2017

REVISED
18 March 2017

ACCEPTED FOR PUBLICATION
12 April 2017

PUBLISHED
17 May 2017

PAPER

Characterization of thin-film adhesion and phonon lifetimes in Al/Si membranes by picosecond ultrasonics

Martin Grossmann[1], **Martin Schubert**[1], **Chuan He**[1], **Delia Brick**[1], **Elke Scheer**[1], **Mike Hettich**[1], **Vitalyi Gusev**[2] **and Thomas Dekorsy**[1,3]

[1] Department of Physics, University of Konstanz, Germany
[2] LAUM, UMR-CNRS 6613, Universit du Maine, Av. O. Messiaen, F-72085 Le Mans, France
[3] Institute for Technical Physics, German Aerospace Center, Pfaffenwaldring 38-40, D-70569 Stuttgart, Germany

E-mail: martin.grossmann@uni-konstanz.de

Keywords: interface adhesion, time domain spectroscopy, phonons, non-destructive testing, intrinsic damping

Supplementary material for this article is available online

Abstract

We quantitatively study interfacial adhesion in a two-layer membrane system consisting of Al and Si with femtosecond time-resolved laser spectroscopy. High-frequency acoustic pulses in the sub-THz regime are utilized to characterize the membrane system. In order to explain the distinct features of the measured data, a spring model for the Al/Si interface is employed. We show that acoustic dissipation in this system needs to be included for accurate modeling of the interface adhesion over a broad frequency range. This modeling approach yields a spring constant of $\eta_{\mathrm{Al-Si}} = 17$ kg nm^{-2} s^{-2}, an acoustic phonon lifetime of $\tau_{\mathrm{Al}} = 68$ ps at 240 GHz in polycrystalline Al and a frequency dependence of the lifetime in Si $\propto \omega^{-1}$ in the frequency range from 50–800 GHz.

Heat dissipation in Si is central to the operation of semiconductor devices [1–3]. This becomes even more challenging due to the miniaturization of all components as the contribution of the boundaries to phonon scattering becomes larger [4–6]. The question of understanding and controlling thermal phonons is of major interest [7–9]. Quantitative values for intrinsic phonon–phonon scattering processes and extrinsic scattering processes due to defects and surface/interface roughness are still under investigation [10–12]. While there exist a wide variety of tools for the spatial mapping of temperature [13, 14], there are not many temporal techniques for measuring nonequilibrium heat transport. One way is to look at coherent acoustic phonons at frequencies that contribute to the spectrum of thermal phonons [15].

Picosecond laser ultrasonics [16, 17] is known to be a powerful tool for the characterization of the elastic properties of thin films. Sub-nanometer thick interfacial layers separating thin films from the substrate can influence both the decay time of the thin film vibration [18] and propagation of the coherent acoustic pulses [19]. Later it was demonstrated that the quantitative evaluation of the thickness of broad interfacial layers [20–24] and the rigidity of thin interfacial bonds [2, 25–29] can be obtained. Here, we study interfacial adhesion as well as damping behavior in two-layer Al/Si-membranes. As a quantitative measure for the interface adhesion, the spring constant of a massless spring model is determined [25].

The investigated system is a 13 nm thick Al film on top of a 350 nm thick Si membrane (see figure 1(a)). Details regarding the fabrication of the membrane are given in [27]. In [27], Al films with different thicknesses were fabricated by sputtering deposition on the membranes, which led to strong adhesion between both layers. Here, in contrast to this approach, the Al film was thermally evaporated, resulting in reduced interface adhesion. The measurements were conducted with an 800 MHz Ti:sapphire pump-probe setup, utilizing the asynchronous optical sampling principle. Further details regarding the setup are given in [27, 30]. We impulsively excite the Al film with an fs-laser pump pulse (30 mW power, 790 nm wavelength) and the response of the sample is measured via a probe pulse (5 mW power, 820 nm wavelength). We neglect generation in Si through the deformation potential, because it appears at frequencies that are considerably lower (<50 GHz [27]) than those of interest to us in the current research (of the order of f_{Al}). A typical transient is shown in

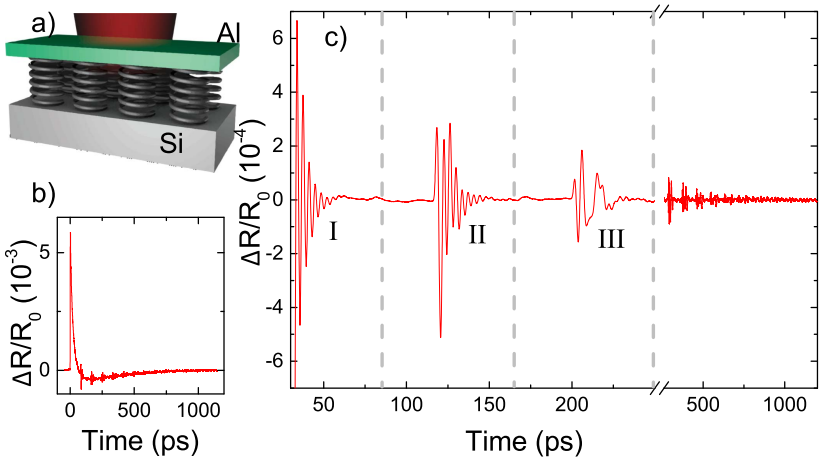

Figure 1. (a) A schematic of the sample: a thin Al film on top of a Si membrane, connected by springs (thickness of layers and springs not to scale). (b) Time-resolved reflectivity changes in the membrane. (c) The extracted phonon signal without background contributions caused by hot electrons. Details of the labeled signal parts are described in the text.

figure 1(b). After a strong rise in reflectivity at a zero time delay, the reflectivity drops again and small features become visible. The sharp rise is due to the ultrafast laser heating of the electrons in the Al, which thermalize via electron–electron and electron–phonon interactions. After subtraction of the electronic background, a coherent phonon signal is obtained (see figure 1(c)). The first 30 ps are dominated by a damped oscillation (I), whereas 88 ps later an acoustic echo emerges (II), which reappears every 88 ps (III,…). Subsequent echoes show changes in their shape and a decrease in their amplitude.

In the following, we will first give a short qualitative explanation of the most salient features. Due to the high reflectivity and short optical penetration depth in Al (∼ 10 nm) at a wavelength of 800 nm, most of the pump light entering the Al film is absorbed. The excited electrons and their relaxation, which provide energy for the Al lattice, induce a homogeneous strain in the Al film [27]. This strain distribution propagates in a direction perpendicular to the surface. Weak adhesion leads to the increased frequency-dependent reflection of the acoustic pulses at the Al/Si interface (equation (2)), which manifests itself as damped oscillation in the transient (I). The launched acoustic pulse, including the reverberations at the interfaces Al/Si and Al/air, then undergoes one round trip in the Si. At the return, it will be detected as the first echo. A part of the pulse will be reflected directly at the Si/Al interface and the rest will be reflected—including reverberations—on the surface of the Al film. The directly reflected part and the part that is transmitted to the Si after the reverberations in the Al film combine after the round trip time $2t_{\mathrm{Al}}$ in the Al. The second echo is detected after an additional round trip in the Si.

In figure 2(a) the Fourier transformations of the oscillating part (I), the first echo (II), the second echo (III), and the whole time transient are shown. The spectrum of the first oscillation (I) shows a maximum at $f_{\mathrm{Al}} = 280$ GHz, which can be attributed to the fundamental acoustic resonance of the Al film. Using $f_{\mathrm{Al}} = v_{\mathrm{Al}}/2h_{\mathrm{Al}}$, where $v_{\mathrm{Al}} = 6430$ m s^{-1} is the longitudinal speed of sound in Al, one obtains $h_{\mathrm{Al}} = 11.5$ nm for the thickness of the Al film, which is in good agreement with the nominal value measured by a crystal oscillator during the evaporation process.

The spectrum of the first echo (II) spans from a few GHz to 800 GHz with a maximum at f_{Al} and two distinct minima at 10 and 460 GHz. The spectrum of the second echo (III) is similar to the spectrum of the first echo, but instead of the maximum at f_{Al} there is a minimum. Finally, the spectrum of the whole time transient has the same shape as the first echo, but additionally exhibits a pronounced comb-like modulation in frequency with the 12 GHz mode spacing. This is due to the resemblance of the system to an acoustic cavity. The frequency spacing between the peaks is given by the inverse round trip time of the total system $t_{\mathrm{RT}} = 2(t_{\mathrm{Al}} + t_{\mathrm{Si}}) = (12\ \mathrm{GHz})^{-1} = 83$ ps, where t_{Al} and t_{Si} are the respective propagation times for a single pass of the acoustic pulse in Al and Si.

In the following, we want to point out the differences between a similar system with perfect adhesion and our data presented here. In figure 3(a), the time domain data of the first 120 ps is shown for a perfectly adhered system [27]. In stark contrast to the weakly adhered system, no eigenmode oscillations of the Al film are visible, which in turn causes a less complicated shape of the first acoustic echo.

In figure 3(b), the spectra of the first echoes including their simulations are shown. Due to the different thicknesses of the samples, a frequency shift between the corresponding spectra is apparent. The important qualitative difference, however, is the shape of the spectral distribution in the region between 50 and 300 GHz.

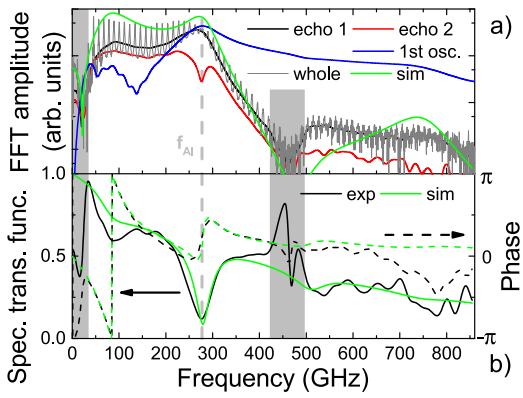

Figure 2. (a) Fourier transformations at the time intervals I, II, III and of the whole time transient on a logarithmic scale (see figure 1(b)). Additionally, the simulation of the first echo is shown. The gray marked areas depict the regions in the spectrum where the spectral amplitude of the echoes is too small to give reliable data. (b) The absolute value and the phase of the extracted spectral transformation function from dividing echo 2 by echo 1, as well as the respective simulated function.

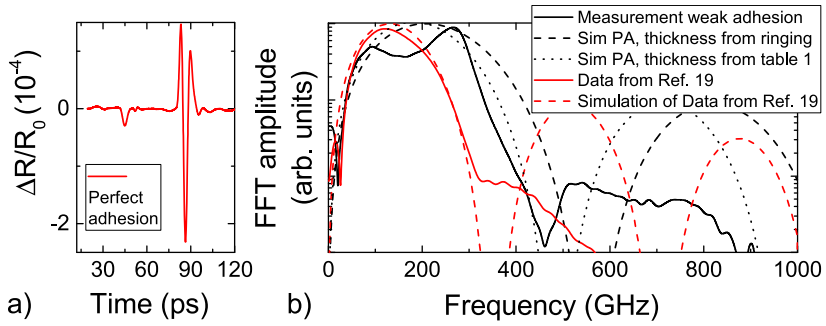

Figure 3. (a) The first 120 ps of the time transient of a perfectly adhered sample. (b) A comparison of the spectrum of the first echo for a perfectly adhered film and the discussed weakly adhered film. Additionally the simulations with assumed perfect adhesion are shown.

Table 1. The parameters used for the simulation.

h_{Al}(nm)	h_{Si}(nm)	τ_{Al}	τ_{Si}	η_{Al-Si} (kg nm^{-2} s^{-2})
13.2	352	$12.6/\omega$	$300/\omega$	17

Here, the curvature of the spectral distribution of the perfectly adhered sample is opposite to the weakly adhered one, i.e. instead of a calculated negative curvature we obtain a positive, and thus dip-like curvature of the spectrum. In [27] we derived the following proportionality for the spectrum of the first pulse, assuming a homogeneous thermoelastic stress distribution as the initial condition: $(\omega_{Al}/\omega)^2 \cdot \sin^4(\pi\omega/2\omega_{Al})$. For reasons of clarity we use the angular frequency ω in the calculations and the frequency $f = \omega/2\pi$ for the numeric values and graphs. This result was obtained by solving the equation of motion for the displacement field of longitudinal acoustic vibrations for the two-layer system and including the generation and detection processes.

While the spectrum of the perfectly adhered sample is well reproduced (only higher frequencies have smaller amplitudes than what is predicted), the result for the spectrum calculated with f_{Al} leads to the wrong positions of the maxima and minima. Using the thickness given in table 1, the agreement is much better, but the dip-like curvature at the position of the maximum still persists.

These differences can be attributed to a weaker interface adhesion between the two layers, which we account for in the modeling by a massless spring. The introduced spring leads to an increased reflectivity between the Al and Si layers with a pronounced frequency dependence. While the reflectivity is close to the case of perfect adhesion at low frequencies, there is an elevenfold increase at 300 GHz. This behavior reproduces the changes in the spectral shape in the case of weak adhesion compared to the case of perfect adhesion. (For more details regarding the calculation of the spectrum see the supplementary section.)

The best theoretical result, taking into account all the aforementioned points, is presented in figure 2(a) as a solid green curve. We used the values given in table 1. We have already achieved good agreement between the model and the spectrum of the first acoustic pulse. It is important to note, however, that this approach relies on several assumptions regarding the excitation and detection mechanisms (details can be found in the supplementary section). This point hinders any further improvement in the modeling process. Thus, in the following we will present a different modeling approach to quantify the interface adhesion which requires less *a priori* knowledge. This novel approach is based on an analysis of the spectral transformation function.

In figure 2(b), the ratio of the spectra of the second and the first echo is shown as a solid black line. It only has values between one and zero. An overall decrease with an increasing frequency and a pronounced dip around f_{Al} are visible. The gray marked areas depict the regions in the spectrum, where the spectral amplitude of the echoes is too small to give reliable data. This leads to the artifact around 460 GHz.

This ratio, independent of the detection method/technique of the acoustic pulses, describes the transformation of the pulse spectrum caused by the round-trip of the pulses in a two-layer membrane. We call it the spectral transformation function (STF) for a round-trip of the acoustic pulse. The derivation is given in the supplementary section. It includes contributions of the whole sample, i.e. the reflections of the Al/air and Si/air interfaces as well as the occurring reverberations. We want to emphasize that the changes between the acoustic pulses are not just given by the frequency-dependent interface reflection, and should thus not be confused with the interface reflection coefficient given in equation (2) below. Our presented experiments, conducted in a unique two-layer membrane, do not allow for the disentangling of intrinsic and extrinsic contributions to the attenuation of the coherent phonons. For this purpose, experiments in membranes with several different thicknesses of composing layers are necessary. This fact leaves the influences of the massless spring as a parameter of the Al/Si interface, the effective damping in the Al and the effective damping in the Si. For the theoretical spectral transformation function this yields

$$\mathrm{STF} = \exp(2\mathrm{i}k_{\mathrm{Si}}h_{\mathrm{Si}}) \cdot \left(1 - \frac{2}{1 + \frac{\mathrm{i}\omega Z_{\mathrm{Si}}}{\eta} - \frac{Z_{\mathrm{Si}}}{Z_{\mathrm{Al}}}\frac{1+\exp(2\mathrm{i}k_{\mathrm{Al}}h_{\mathrm{Al}})}{1-\exp(2\mathrm{i}k_{\mathrm{Al}}h_{\mathrm{Al}})}}\right) = T \cdot R \tag{1}$$

where k_{Al}, k_{Si} are the complex acoustic wavevectors, whose imaginary parts account for both intrinsic and extrinsic losses, h_{Al}, h_{Si} are the thicknesses, Z_{Al}, Z_{Si} are the complex acoustic impedances of Al and Si, respectively, and η is the real-valued spring constant per unit area. The imaginary part of the wave vector is equal to the effective acoustic attenuation α and is related to the lifetime via $\tau = 1/(v\alpha)$, where v is the longitudinal sound velocity. The right-hand side of the equation consists of two parts: T corresponds to the coefficient of transmission through Si, which is only governed by intrinsic damping as we disregard scattering at the Si/air interface, and R describes the reflection of the acoustic pulse at the Si/Al interface for a pulse coming from the Si side.

We tested several models for phonon damping in the layers, namely constant damping, $1/\omega$ and $1/\omega^2$ decay. The best fit is obtained by the assumption of $1/\omega$ decay in both the Al and Si layers. The absolute value and the phase of the STF of equation 1 are plotted as solid and dotted green lines in figure 2(b). The parameters used are given in table 1. Both the absolute value and phase match well with the measured data up to around 700 GHz. We want to note that only the frequency region, which is not colored in gray, is of relevance for the fitting.

In the following we will not only discuss the influence of the different attenuation processes, but also of the spring constant on the STF. We see from equation (1) that the effects from the attenuation in Si and Al can be separated. Thus T only depends on τ_{Si} while R only depends on τ_{Al} (the damping is included in the wavevectors and in the impedances of each layer). We find that the effect of the imaginary part of the impedance of Si in R is negligible compared to the contributions of the effective attenuation in Al and the spring constant. In figures 4(a)–(b) the spectral transformation functions of Si and Al are plotted for a variety of parameters. The attenuation parameters for the $1/\omega$ decay were changed by $\pm 30\%$. In figure 4(a) we plot the behavior of T depending on the attenuation in the Si. Strongly monotonous behavior which is directly proportional to the damping behavior is seen. The slightly smaller and larger values lead to different slopes compared to the one using the simulation values (black curve), while the $1/\omega^2$ decay and the constant decay have very different slopes.

In figure 4(b) we plot R with the spring constant value η given in table 1. Contrary to the behavior of T, only a weak frequency dependence of R is apparent. Distinct minima at 100 GHz, 280 GHz and 510 GHz arise in the spectral transformation function. The changes caused by the $1/\omega$ decay with a $\pm 30\%$ variation make the dips smoother or sharpen them compared to the slope given by the simulation values (black curve). Also, the smaller minimum at 100 GHz becomes more pronounced. For the $1/\omega^2$ decay, the minimum at 100 GHz vanishes while for constant attenuation the dips at higher frequencies become more pronounced. The frequency spacing between the individual dips is determined by the relation $v_{\mathrm{Al}}/2h_{\mathrm{Al}}$.

In figure 4(c), the variation of the STF with the spring constant is shown, while $\tau_{\mathrm{Si,Al}}$ have the values given in table 1. Here, variations by $\pm 30\%$ lead to a frequency shift in the dips. Stronger adhesion leads to a blue shift and

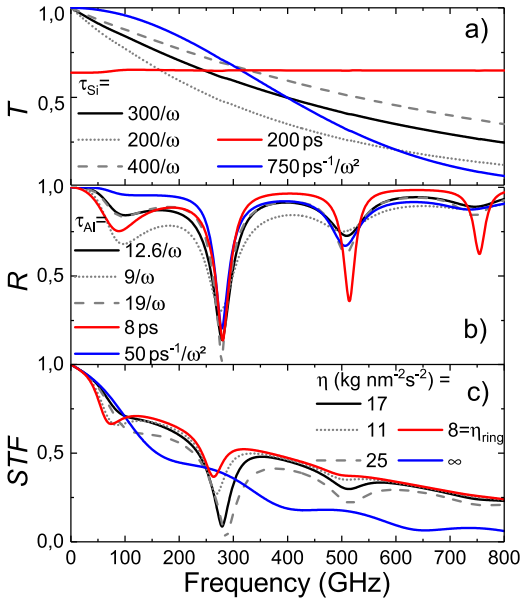

Figure 4. (a) The simulated spectral transformation function for the Si layer; three different lifetime behaviors are used ($1/\omega$, $1/\omega^2$, const). (b) The simulated spectral transformation function for the Al layer; three different lifetime behaviors are used ($1/\omega$, $1/\omega^2$, const). (c) The total simulated spectral transformation function for different spring constants.

weaker adhesion leads to a red shift. For the extreme case of perfect adhesion ($\eta = \infty$) the dips are smoothed because only the impedance mismatch leads to a reflection at the interface and therefore the resonance is smaller. For no adhesion ($\eta = 0$) no acoustic pulse would be transmitted into the Si, and thus only a ring down of the Al film oscillation would be observed in the experiment. This would correspond to no incoming wave in our system and therefore to $R = \infty$. The black line corresponds to the values in table 1.

From the results we can see that the overall decay is mainly given by the damping in the Si, while the spacing of the dips is given by the eigenmodes of the Al film, and the amplitudes of the minima by the attenuation; the frequency shift and weaker change of the amplitudes of the minima (compared to the attenuation of the Al) is determined by the spring constant.

Recent results in sputtered Al for acoustic attenuation are $\alpha_{\mathrm{Al}} = 8900\ \mathrm{cm}^{-1}$ at 30 GHz and $\alpha_{\mathrm{Al}} = 20500\ \mathrm{cm}^{-1}$ at 50 GHz [31]. This corresponds well to our values, where we find $\alpha_{\mathrm{Al}} = 23000\ \mathrm{cm}^{-1}$ at 240 GHz. Additionally the Si attenuation values correspond well to the literature values of the Si membranes, where the behavior of $\tau_{\mathrm{Si}} = 300/\omega$ is an upper boundary for the data of Cuffe *et al* [11]. As the proposed damping mechanism in [11] is governed by surface roughness, and we exchange one surface with the Al layer, it seems reasonable to obtain a slightly weaker effective dissipation in the Si in our experiments.

Our value for the spring constant of $\eta = 17\ \mathrm{kg\ nm}^{-2}\ \mathrm{s}^{-2}$ is similar to the value found for a gold film on the Si substrate of $\eta_{\mathrm{Au-Si}} = 13\ \mathrm{kg\ nm}^{-2}\ \mathrm{s}^{-2}$ [25] and the value of Al on Si by Antonelli *et al* of $\eta_{\mathrm{Al-Si}} = 6\ \mathrm{kg\ nm}^{-2}\ \mathrm{s}^{-2}$ [2]. But in those measurements, the extraction of the spring constant was done differently and no dissipation was included in the metals. The oscillation at the beginning of the measurement was assumed to be the fundamental eigenmode frequency ω_{Al} of the metal film, neglecting higher order modes, and to be governed by the increased reflectivity due to the spring:

$$r_{\mathrm{Al-Si}} = \frac{Z_{\mathrm{Al}} - Z_{\mathrm{Si}} + \mathrm{i}Z_{\mathrm{Al}}Z_{\mathrm{Si}}\omega_{\mathrm{Al}}/\eta_{\mathrm{ring}}}{Z_{\mathrm{Al}} + Z_{\mathrm{Si}} + \mathrm{i}Z_{\mathrm{Al}}Z_{\mathrm{Si}}\omega_{\mathrm{Al}}/\eta_{\mathrm{ring}}}. \tag{2}$$

Here, we neglect attenuation in the Al and just fit the oscillation (I) with a damped sine and get $\Gamma = 30$ ps for the decay rate. The relation between the analytical formula (equation (2)) and the measured decay is $r = \exp(-\Gamma\omega_{\mathrm{Al}})$. With this approach we evaluate for the spring constant of part (I) $\eta_{\mathrm{ring}} = 8\ \mathrm{kg\ nm}^{-2}\mathrm{s}^{-2}$, which is half the value we get from the simulation with equation (1). However, it is in very good agreement with the value by Antonelli *et al* ($\eta = 6\ \mathrm{kg\ nm}^{-2}\mathrm{s}^{-2}$) [2], where they also neglected the attenuation in Al. Further below we will discuss the case of evaluating the spring constant including adhesion and attenuation from the oscillating part at the beginning (I).

The above considerations show that our approach gives us access not only to important information on the interfacial adhesion but also to the effective acoustic damping behavior in the respective layers. Furthermore, this approach circumvents the usual problems in the analysis caused by the excitation and detection process, which would require us to model the spectrum or (via the inverse Fourier transformation) the time transient.

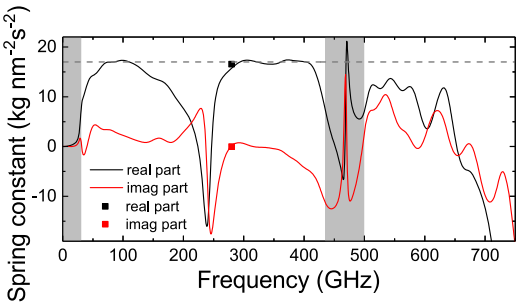

Figure 5. The calculated spring rigidity from the spectral transformation function with the parameters given in table 1. Solid lines: evaluated from the spectral transformation function; dots: evaluated from the ringing at the beginning of the measurement. The dashed gray line shows the constant value used in the simulation. The gray marked areas depict the regions where the spectral amplitude of the echoes is too small to give reliable data.

Thus, only the parameters given in table 1 enter the final simulation. We think it is worth mentioning that the adhesion is potentially mediated by a nanometric layer of SiO_2. In the supplementary section, we derive a model for the spectrum by including simplified excitation and detection processes and we see that the simulated spectrum of the first echo is overestimated around 100 GHz, see figure 2(a).

It is possible to invert equation (1) and extract the spring constant from the measurement. For the whole range of frequencies, where the spectral transformation function measurement is available, we obtain:

$$\eta = \mathrm{i}\omega Z_{\mathrm{Al}}\left[\frac{1+\mathrm{e}^{2\mathrm{i}k_{\mathrm{Al}}h_{\mathrm{Al}}}}{1-\mathrm{e}^{2\mathrm{i}k_{\mathrm{Al}}h_{\mathrm{Al}}}} - \frac{Z_{\mathrm{Al}}}{Z_{\mathrm{Si}}}\frac{R+1}{R-1}\right]^{-1}. \tag{3}$$

The calculated frequency-dependent spring constant is plotted in figure 5. We need to adjust the measured value by the damping of the Si, as only R is important in equation (3). The spring rigidity is constant for the whole regime of the STF, but there is a pronounced dip at a slightly smaller frequency than the undamped eigenmode frequency of the Al film. If we compare the frequency range of the dip with the results from figure 2(b), we see that the absolute value and phase between the experiment and simulation (where we assumed a frequency-independent spring constant) have a slight deviation at exactly this frequency range between 150–300 GHz. Thus, the deviation in the spring constant in figure 5 from the frequency-independent behavior is caused by the discrepancy between the measured and the modeled data. This also shows that the evaluation of the spring behavior is a very sensitive measure of the modeling quality. We want to mention that this approach also enables us to obtain values for a complex spring rigidity. In principle, it is possible to include dissipation through the imaginary part of the spring in the modeling, but the best results (including the inverse check with equation (3)) are obtained with only a real-valued spring constant, indicating that damping through the interfacial bonds can be neglected.

There exists an alternative approach for extracting the spring constant directly from the measurement data, which allows us to corroborate our calculations. In equation (3) we set R to infinity (which corresponds to no incoming wave in the system), and use the frequency f_{Al} and the decay rate $\Gamma = 30$ ps taken from fitting the ringing at the beginning of the time transient. The result for the spring constant extracted at f_{Al} is shown in figure 5. Good agreement between the real and imaginary part is obtained by this approach and the spring constant evaluated over the whole frequency range is found. The results of both approaches are strongly dependent on the thickness and attenuation in the Al.

To examine the quality of the theory and our assumptions, besides the simulation of the first echo shown in figure 2(a), we simulate the measurement data in the time domain in figure 6 with the values of table 1. We used homogeneous excitation and homogeneous detection in the Al film (the details are given in the supplementary section). A good agreement between the measurement and simulation can be seen. Furthermore, the simulation with the frequency-independent spring constant η_{ring} is shown. For the first echo the minimum is still not reproduced. For the second echo no resemblance to the measured data is visible anymore. This confirms the reasoning for our detailed approach.

To conclude, we showed that we are able to quantitatively determine the interfacial adhesion in a layered membrane system consisting of Al and Si. The existence of high-frequency acoustic pulses in the system allows us to extract information about the interfacial adhesion ($\eta = 17$ kg nm^{-2} s^{-2}) and the acoustic damping behavior in the respective layers over a wide frequency range from a few GHz to 700 GHz. Our approach does not require knowledge about the excitation or detection processes in the sample and thus eliminates a potential error source. A simple spring model is sufficient for modeling distinct characteristics of the measured data. Our findings regarding the interfacial adhesion are in good agreement with the literature results from Antonelli *et al*

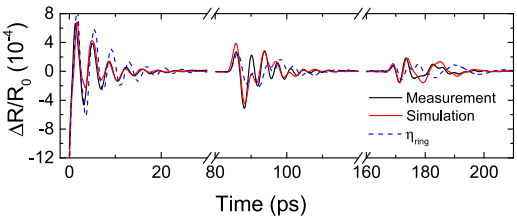

Figure 6. A time domain simulation of the measurable data compared to the measured data. The parameters used are given in table 1. Additionally the simulation with the spring constant η_{ring} evaluated from the ringing due to the reflection at the interface only is shown.

[2], when we also neglect the attenuation in Al. The damping we obtain for polycrystalline Al is in good agreement with the results from Bryner *et al* [31], and the values for the damping in Si are in good agreement with the findings of Cuffe *et al* [11]. Our results show that this usual approach, which neglects acoustic damping, can cause considerable deviations in the interfacial adhesion, and should thus be included in the modeling when quantitative measurements are aimed for.

Acknowledgments

This work was supported by the German Research Foundation (DFG) through SFB 767. Chuan He gratefully acknowledges the financial support from the China Scholarship Council (CSC).

References

[1] Chen W and Maris H 1994 *Phil. Mag.* B **70** 687
[2] Antonelli G A, Perrin B, Daly B C and Cahill D G 2006 *MRS Bull.* **31** 607
[3] Ward A and Broido D A 2010 *Phys. Rev.* B **81** 1
[4] Pop E, Sinha S and Goodson K 2006 *Proc. IEEE* **94** 1587
[5] Bodapati A, Schelling P, Phillpot S and Keblinski P 2006 *Phys. Rev.* B **74** 245207
[6] Franklin A D 2015 *Science* **349** 6249
[7] Maldovan M 2013 *Nature* **503** 209
[8] Maasilta I and Minnich A J 2014 *Phys. Today* **67** 27
[9] Volz S *et al* 2016 *Eur. Phys. J.* B **89** 15
[10] Maznev A A, Hofmann F, Jandl A, Esfarjani K, Bulsara M T, Fitzgerald E A, Chen G and Nelson K A 2013 *Appl. Phys. Lett.* **102** 041901
[11] Cuffe J *et al* 2013 *Phys. Rev. Lett.* **110** 095503
[12] Maznev A, Hofmann F, Cuffe J, Eliason J and Nelson K 2015 *Ultrasonics* **56** 116
[13] Christofferson J, Maize K, Ezzahri Y, Shabani J, Wang X and Shakouri A 2008 *J. Electr. Packag.* **130** 41101
[14] Mecklenburg M, Hubbard W A, White E R, Dhall R, Cronin S B, Aloni S and Regan B C 2015 *Science* **347** 629 LP
[15] Cahill D G, Ford W K, Goodson K E, Mahan G D, Majumdar A, Maris H J, Merlin R and Phillpot S R 2003 *J. Appl. Phys.* **93** 793
[16] Thomsen C, Strait J, Vardeny Z, Maris H J, Tauc J and Hauser J J 1984 *Phys. Rev. Lett.* **53** 989
[17] Thomsen C, Grahn H, Maris H and Tauc J 1986 *Phys. Rev.* B **34** 4129
[18] Tas G, Stoner R J, Maris H J, Rubloff G W, Oehrlein G S and Halbout J M 1992 *Appl. Phys. Lett.* **61** 1787
[19] Wright O B and Kawashima K 1992 *Phys. Rev. Lett.* **69** 1668
[20] Bonello B, Armand F, Pradeau J-P, Perez H, Perrin B and Louis G 1999 *J. Appl. Phys.* **86** 4959
[21] Bonello B, Louis G and Battioni P 2003 *Rev. Sci. Instrum.* **74** 889
[22] Hettich M *et al* 2011 *Appl. Phys. Lett.* **98** 261908
[23] Hettich M, Jacob K, Ristow O, He C, Mayer J, Schubert M, Gusev V, Bruchhausen A and Dekorsy T 2012 *Appl. Phys. Lett.* **101** 191606
[24] Hettich M, Jacob K, Ristow O, Schubert M, Bruchhausen A, Gusev V and Dekorsy T 2016 *Sci. Rep.* **6** 33471
[25] Tas G, Loomis J J, Maris H J, Bailes A A and Seiberling L E 1998 *Appl. Phys. Lett.* **72** 2235
[26] Pezeril T, Chigarev N, Mounier D, Gougeon S, Ruello P, Breteau J M, Picart P and Gusev V 2008 *Eur. Phys. J.: Spec. Top.* **153** 207
[27] Grossmann M *et al* 2013 *Phys. Rev.* B **88** 205202
[28] Yang N, Luo T, Esfarjani K, Henry A, Tian Z, Shiomi J, Chalopin Y, Li B and Chen G 2015 *J. Comput. Theor. Nanosci.* **12** 168
[29] Beardsley R, Akimov A V, Greener J D G, Mudd G W, Sandeep S, Kudrynskyi Z R, Kovalyuk Z D, Patanè A and Kent A J 2016 *Sci. Rep.* **6** 26970
[30] Bartels A, Cerna R, Kistner C, Thoma A, Hudert F, Janke C and Dekorsy T 2007 *Rev. Sci. Instrum.* **78** 035107
[31] Bryner J, Kehoe T, Vollmann J, Aebi L, Wenke I and Dual J 2010 *Phys. Procedia* **3** 343